Green Fabrication, Characterization, and Photocatalytic Study of Ag-Au Bimetallic Nanocomposite

Arunkumar Lagashetty

arun.lagashetty@gmail.com

Vijayanagara Sri Krishnadevaraya University

N Nandini

Vijayanagara Sri Krishnadevaraya University

U Sharanabasava

Vijayanagara Sri Krishnadevaraya University

B Sahana

Vijayanagara Sri Krishnadevaraya University

Roja B. M

Vijayanagara Sri Krishnadevaraya University

V Veena

Ballari Institute of Technology and Management

B. Umareddy

Vijayanagara Sri Krishnadevaraya University

Article

Keywords: Green synthesis, Ag-Au BMNPs, Bacopa monnieri, Photocatalytic degradation, Methylene blue

Posted Date: April 13th, 2026

DOI: https://doi.org/10.21203/rs.3.rs-9065757/v1

Additional Declarations: No competing interests reported.

Abstract

Green plant materials in the form of extract support the bio-reduction reaction as reducing and capping agents. The present work reports the synthesis of Ag-Au bimetallic nanoparticles (BMNPs) using *Bacopa monnieri* leaf extract as a precursor, with $AgNO_3$ and $AuCl_2$ as source metals. Specifically, silver and gold bimetallic nanoparticles (Ag-Au BMNPs) are synthesised by bio-reduction method using *Bacopa monnieri* leaf extract. The extract serves as a reducing, stabilizing, and capping agent for the effective green synthesis of said nanoparticle. The synthesized Ag-Au BMNPs was characterized by various analytical tools for its phase formation. FT-IR spectral analysis confirms the bio-derived Ag-Au BMNPs with absorption below 1000 cm^{-1}. The UV-Visible spectra show a strong absorption peak at 650 nm, which is the characteristic absorption of green-synthesized Ag-Au BMNPs. The XRD study confirms the validation of standard characteristics by crystalline phase formation. Scanning electron microscopic (SEM) and energy dispersive X-ray microanalysis (EDX) confirm the spherical morphology with some agglomeration and the presence of Ag and Au elements. Dynamic light scattering (DLS) indicates average particle sizes of 51 nm and 668 nm with a polydispersity index (PDI) of 5.1 and 94.9, suggesting moderate polydispersity. Raman and fluorescence studies further validate the structure and photonic potential. The photocatalytic activity was evaluated for methylene blue (MB) dye degradation, showing significant reduction over 60 minutes under light exposure. Results indicate excellent photocatalytic performance, highlighting potential for environmental remediation. This green approach emphasizes sustainability, biocompatibility, and cost-effectiveness.

1. Introduction

With the development of human society, water pollution has caused a tremendous negative impact on human life and social development [1–4]. Acid, alkali, metal compounds and organic dyes in sewage are the primary sources of pollution, and sewage treatment methods mainly include physical adsorption, biodegradation and photo catalytic [5–7]. Photo catalysis is a reaction process in which organic pollutants are oxidized and degraded under visible or ultraviolet light. It is necessary to improve the degradation ability of photo catalyst. So far, most of the researches have designed photo catalyst modifying its properties by doping, constructing hetero junction, and compounding with carbon materials. The modification of semiconductors by introducing precious metals improved the charge separation and promoted the charge transfer process [8, 9].

In general, the enhancement of photo catalyst by noble metal nanoparticles has two main aspects. First, precious metal nanoparticles can act as electron traps to capture photo generated electrons from semiconductors, leading to the efficient separation of electron-hole pairs. Secondly, the surface plasmon resonance effect of electrons in noble metal nanoparticles enables them to have high absorption capacity in the visible region, which can promote the generation and separation of electron-hole pairs in semiconductors [10, 11]. Noble metal nanoparticles (NPs) have widespread uses in several technological applications [12–14] and various wet chemical synthesis methods have been reported. Bimetal-based noble nanomaterials integrate two or more distinct functionalities into a single entity, thereby obtaining superior and sometimes unprecedented properties. Compared with the individual components, bimetallic nanostructures comprise a new class of materials with unique physicochemical properties [15–17]. BMNPs are more attractive from a scientific and technological viewpoint as compared to monometallic (NPs) due to their superior characteristics. BMNPs are composed of two different metals with enhanced electronic, plasmonic, catalytic, optical, thermal, magnetic and biological properties due to a synergistic effect [18].

Traditional chemical synthesis routes rely on hazardous reductants and stabilizers, generating toxic by-products and increasing costs. In contrast, green synthesis using plant extracts provides an eco-friendly and biocompatible alternative. Plant based phytochemicals such as polyphenols, flavonoids, terpenoids, and alkaloids act as natural reducing, capping, stabilizing agents and facilitating bio-reduction reaction. The synthesis of BMNPs via green route is gaining particular attention in reducing the unwanted waste products which are hazardous to human health and the environment [19, 20]. In this direction, many researchers have been trying to develop a modified green route for the effective and rapid fabrication of BMNPs with higher dispersion and uniformity. Various methods have emerged for the fabrication of noble BMNPs by following green chemistry principles [21, 22]. For example, polyphenols can chelate with metal ions in solution and further reduce them to the corresponding metal [23]. In fact, many plant extracts are rich in polyphenols have been employed extensively as environmentally friendly alternatives to chemical and physical methods for the synthesis of noble BMNPs.

The escalating environmental pollution from synthetic organic dyes, such as MB discharged by textile and other industries, poses severe threats to aquatic ecosystems and human health due to their toxicity, carcinogenicity, and persistence in water bodies. Conventional treatment methods often prove inadequate for complete mineralization, driving the need for advanced, sustainable remediation technologies like visible-light photo catalysis, which harnesses solar energy to generate reactive oxygen species for efficient dye degradation. Noble metal nanoparticles, particularly silver (Ag) and gold (Au), exhibit exceptional plasmonic properties that enhance light absorption and charge separation in photo catalytic processes [24]. Ag-Au BMNPs offer synergistic advantages over monometallic counterparts, including tunable surface plasmon resonance, improved stability against oxidation, reduced aggregation, and superior catalytic performance arising from modified electronic structures and alloying effects. These attributes make Ag-Au BMNPs promising for environmental applications, including dye degradation were selected as photo catalyst for the current study. *Bacopa monnieri* (Brahmi), an Ayurvedic herb renowned for its nootropic, antioxidant, and neuroprotective properties, is rich in bioactive compounds including bacosides (triterpenoid saponins), flavonoids, and other secondary metabolites. These phytochemicals enable the formation of effective mediation of metallic nanoparticle. However, its application in synthesizing Ag-Au BMNPs remains underexplored, representing a novel bridge between traditional herbal medicine and sustainable nanotechnology.

The present study reports the green synthesis of Ag-Au BMNPs via biological reduction using *Bacopa monnieri* leaf extract, which serves as a multifunctional precursor. The nanoparticles were characterized using various characterisation tools. Their photocatalytic efficacy was evaluated against MB degradation under light exposure, revealing excellent performance attributable to plasmonic synergy and efficient reactive species generation. This approach underscores sustainability, cost-effectiveness, and biocompatibility, with potential for scalable environmental remediation.

2. Materials and Methods

Plant mediated reduction method was used for the synthesis of Ag-Au bimetallic nanoparticles. *Bacopa monnieri* plant fresh leaves were collected in early morning from a botanical garden, Vijayanagara Sri Krishnadevaraya University, Ballari. The *Bacopa monnieri* plant leaf extract was prepared. Chemicals used are AR grade and double distilled water for the preparation of solution and extract. Biological reduction method was used for the synthesis of Ag-Au BMNPs.

This study adheres to all applicable institutional, national, and international guidelines for plant research. *Bacopa monnieri* (L.) Wettst. Leaves were collected from the VSKU Botanical Garden, Bellary, Karnataka, India, with permission from the Botanical Garden Management Committee. No wild or endangered species were involved (*Bacopa monnieri*: IUCN Least Concern; not CITES-listed). Voucher specimens No. HDUD 528, identified by Dr. Haleshi C (Assistant Professor, Department of Studies in Botany, Davangere University, Karnataka, India), are deposited in the Davangere University, Botany Herbaria (publicly accessible).

2.1 Preparation of extract

50 grams of leaves were carefully selected, avoiding any damaged or diseased parts, and thoroughly washed under running distilled water to remove dust, soil, and potential contaminants. The cleaned leaves were then crushed using a mortar and pestle to break down the cellular structure and facilitate extraction of intracellular components. The crushed biomass was transferred to a 100 mL conical flask containing 50 mL of distilled

water, creating a 1:1 ratio of plant material to solvent for optimal extraction efficiency. The mixture was heated on a hot plate with magnetic stirring at 80°C for 15 minutes to promote the release of reducing agents from plants into the aqueous phase. The mixture was allowed to cool to room temperature, during which occasional stirring was applied to enhance diffusion. Filtration the content using Whatman filter paper No. 42, which has a pore size of 2.5 µm, suitable for retaining plant debris while allowing the passage of soluble extracts. Eluent is collected as a plant extract for synthesis of Ag-Au BMNPs. The complete extract preparation is shown in Fig. 1(a-d) respectively.

Figure 1: a) *Bacopa monnieri* plant leaves b) Crushed plant leaves c) Boling of extract d) Filtering of leaf extract

2.2 Synthesis of Ag-Au BMNPs

Silver nitrate ($AgNO_3$, 0.01 M) and gold chloride ($AuCl_2$, 0.01 M) solutions were prepared double distilled water. A known volume of prepared *Bacopa monnieri* leaf extract (Fig. 2(a)) was mixed carefully with equal volume of 0.01M AuCl4 and $AgNO_3$ solution as shown in Fig. 2(b). The addition was done drop wise under constant stirring (500 rpm) using a magnetic stirrer to ensure homogeneous mixing. These metal salts serve as precursors for Ag^+ and Au^{3+} ions, respectively. The reaction mixture was heated up to 70^0C and later cooled to room temperature for 24 hours for complete reduction. Heating facilitates the reduction kinetics by increasing molecular collisions and activating phytochemical reducing agents. The formation of Ag-Au BMNPs was confirmed as the colour changes to grey initially as nucleation starts and later changes to purple after complete reduction (Fig. 2(c)). Reaction suspension product was centrifuged at 6000 rpm for 10 minutes using a high-speed centrifuge (Remi, India) to separate the nanoparticles from its supernatant liquid. The precipitate was washed thrice with distilled water to remove unreacted ions and excess extract, and then redispersed in ethanol for recrystallization. The final product was dried under vacuum at 40°C for 12 hours to obtain powdered Ag-Au BMNPs (Fig. 2(d)). This method adheres to green principles, using no toxic reductants and producing minimal waste.

2.3 Photo catalytic degradation of dye:

Usually, a stock solution of 1000 mL of double-distilled water was mixed with 10 mg of methylene blue dye. A 100 mL solution of methylene blue dye was mixed with roughly 10 mg of biosynthesized Ag-Au BMNPs. Additionally, a control group without any Ag-Au BMNPs was kept. To ensure that the working solution was in equilibrium, the reaction suspension was thoroughly mixed by magnetically stirring it for 30 minutes prior to exposure to radiation. The dispersion was then exposed to sunlight and observed from dawn to dusk. Aliquots of 2–3 mL suspension were filtered at predetermined intervals and utilized to assess the dye's photo catalytic degradation. A UV-Vis spectrophotometer was then used to measure the supernatant's absorbance spectrum at various wavelengths. The dye concentration during degradation was computed by the absorbance value at 650 nm [25].

2.4 Analytical techniques

This solution's UV-Vis spectrum was captured in DMSO solution using a Shimadzu UV-1800 instrument, which worked in the 400–800 nm wavelength range. Perkin Elmer tool with KBr pellet technique, the FT-IR spectra was obtained in the mid-IR region of 400–4000 cm^{-1}. The XRD method was used to ascertain the nanoparticles' crystalline structure. The XRD pattern was obtained using computer controlled XRD-system. JEOL, Model: JPX-8030 with Cu Kα radiation (Ni filtered = 13,418 A°) at the range of 40kV, 20A tool is used. A 0.22-liter syringe-driven filter unit was used to filter the generated nanoparticles' aqueous solution, and Nano-Zeta-Sizer was used to estimate the hydro dynamic diameter (HDD) of the dispersed nanoparticles using the dynamic light scattering (DLS) principle. Scanning electron low and high resolution (Zeiss EVO) was used to examine the surface morphology of the Ag-Au BMNPs samples at magnifications ranging from 10 to 600,0000 while operating at an accelerating voltage of 30 kV. SEM coupled with EDX was reported.

3. Results and Discussion

3.1 FT-IR Analysis

Figure 3 shows FT-IR spectra of the prepared bimetallic Ag-Au BMNPs. It shows a broad peak at 3381 cm^{-1} (-OH, moisture), peaks at 2967 cm^{-1}, 2427 cm^{-1}, and 2233 cm^{-1} correspond to C ≡ C stretching vibrations, indicating the presence of alkyne or nitrile groups, possibly from secondary metabolites in the extract that act as capping agents. The absorptions at 1770 cm^{-1}, 1737 cm^{-1}, and 1509 cm^{-1} are assigned to C = C stretching modes, suggestive of aromatic rings or conjugated systems from flavonoids and bacosides in *Bacopa monnieri*, which are known to reduce metal ions and stabilize nanoparticles through π-electron interactions. A distinctive peak at 877 cm^{-1} represents metal-oxygen bonds (Au-O or Ag-O), arising from oxide layers or coordination with oxygen-containing functional groups from the extract. The band at 670 cm^{-1} indicates the presence of a covalent metal-metal bond (Ag-Au), confirming the bimetallic nature of the alloy. These low-frequency peaks ($<$ 1000 cm^{-1}) validate the bio-derivation, as they align with literature on plant-mediated syntheses where phytochemicals form a protective corona around nanoparticles, enhancing stability and preventing agglomeration [26, 27]. Biologically derived BMNPs spectra show fewer impurity peaks, highlighting the purity of the green method. This functional group analysis elucidates the mechanism: electron donation from phytochemicals to metal ions, followed by nucleation and growth into alloyed structures. This confirms capping by plant phytochemicals and BMNP formation.

3.2 UV-Visible Spectroscopy

UV-Visible spectroscopy was employed to monitor the formation and optical properties of the Ag-Au BMNPs. As depicted in Fig. 4, a prominent absorption peak at 650 nm indicates n-π* transition, confirming Ag-Au alloy formation. This aligns with literature on bimetallic systems [28]. This red-shifted peak compared to monometallic Ag (≈420 nm) or Au (≈520 nm) indicates the formation of a bimetallic alloy rather than a core-shell structure, where electronic interactions between Ag and Au modify the band structure, leading to a single SPR band. The peak's intensity and sharpness suggest good dispersion and uniform size distribution, with no secondary peaks implying high purity and absence of unreduced ions. The SPR position aligns with theoretical predictions for Ag-Au alloys, where the dielectric function shifts with composition ratio [29]. This optical characterisation not only confirms BMNP formation but also highlights their potential in sensing and catalysis, where tunable SPR is advantageous.

3.3 EDX Analysis

EDX pattern of prepared Ag-Au BMNPs is shown in Fig. 5 and obtained data is tabulated in inset table of the figure. The pattern provides the elemental composition of the green-synthesized Ag-Au BMNPs confirming the successful incorporation of both Ag and Au along with surface oxygen [30]. The observed table show Ag as the dominant metallic component with 79.34 wt% (54.94 at%), Au at 11.98 wt% (4.54 at%), and oxygen at 8.68 wt% (40.51 at%). The high atomic percentage of oxygen, despite its lower weight contribution, is typical for light elements and arises primarily from oxygen-containing functional groups (such as hydroxyl and carbonyl) in the phytochemicals from *Bacopa monnieri* leaf extract that cap and stabilize the nanoparticles, as well as minor surface oxidation of the metals. The Ag:Au ratio deviates from the intended 1:1 precursor stoichiometry due to differences in reduction kinetics leading to preferential Ag reduction and an Ag-rich alloy [31, 32]. Importantly, no residual elements from the precursors are detected, indicating effective purification during synthesis. This composition validates the formation of a true bimetallic alloy structure consistent with the single surface plasmon resonance peak at 650 nm in UV-Vis and the intermediate FCC lattice in XRD. The presence of oxygen highlights the role of plant-derived biomolecules in providing a biocompatible capping layer that enhances colloidal stability and supports for photo catalytic activity.

3.4 Raman Spectroscopy

Raman spectroscopy, conducted using 532 nm laser excitation, was employed to examine the molecular structure, bonding, and surface characteristics of prepared Ag-Au BMNPs and is shown in Fig. 6. It reveals two prominent peaks: one at 1586 cm^{-1}, assigned to the G-band arising from graphitic carbon stretching in aromatic rings of biomolecule-derived capping agents, and a low-frequency peak at 144 cm^{-1}, attributed to metal-oxygen vibrations (Au-O or Ag-O) involving sub-surface oxygen species. This low-frequency mode, likely amplified by surface-enhanced Raman scattering (SERS) due to the plasmonic properties of the Ag-Au BMNPs, indicates sub-surface oxygen that could facilitate molecular oxygen adsorption and enhance photo catalytic oxidation processes [33, 34]. The absence of a D-band near 1350 cm^{-1} signifies an ordered, low-disorder capping layer, promoting nanoparticle stability. Strong broad peak at ~ 1350–1600 cm^{-1} (maximum at 1550 cm^{-1}) is the dominant feature and corresponds to the G-band and D-band. It indicates the presence of residual organic capping agents or carbon-containing molecules from the plant extract used in the green synthesis.

3.5 DLS Analysis

The size distribution by intensity graph from DLS analysis depicts the hydrodynamic diameter distribution of the green-synthesized Ag-Au BMNPs in aqueous suspension, measured using a Nano-Zeta-Sizer instrument. Figure 7 shows the DLS spectrum of as prepared Ag-Au BMNPs. In intensity-weighted DLS, larger particles dominate the signal due to scattered light intensity scaling approximately with the sixth power of diameter, making the plot sensitive to aggregates even if present in low numbers. The displayed bimodal profile shows a prominent major peak with maximum intensity around 6–6.5% cantered near 100–200 nm representing the primary population of dispersed nanoparticles, alongside a minor shoulder/peak at lower sizes (~ 50–100 nm with ~ 1–2% intensity) and an extended tail toward larger diameters up to ~ 1000 nm or beyond. This distribution indicates moderate polydispersity, where the main peak corresponds to individual or lightly clustered Ag-Au BMNPs [35]. while the secondary features and rightward tail arise from agglomerates formed by van der Waals attractions, and insufficient steric/electrostatic stabilization in concentrated samples. The negative zeta potential (typically from carboxylate or phenolate groups in *Bacopa monnieri* capping agents) provides electrostatic repulsion to mitigate extensive aggregation, supporting overall nanoscale suitability for applications like photo catalysis [36].

3.6 XRD Analysis

XRD characterisation was employed to investigate the crystalline structure and phase purity of the prepared Ag-Au BMNPs, using Cu Kα radiation (λ = 1.5406 Å) over 2θ range 10–80°. Figure 8 is the XRD pattern of green derived Ag-Au BMNPs, which shows intense Bragg's reflections at 2θ values corresponding to (111), (200), (220), and (311) planes, characteristic of face-cantered cubic (FCC) structure. The peaks here are intermediate between those of pure Ag (JCPDS 04-0783) and Au (JCPDS 04-0784), confirming formation of BMNPs with lattice parameters ≈ 4.08 Å, indicative of solid solution. Crystallite size, calculated via Scherrer equation ($D = K\lambda / \beta \cos\theta$, $K = 0.9$), was ≈ 45 nm, matching DLS primary size. No oxide or impurity peaks were observed in the pattern validate purity of the sample. This crystallinity enhances charge carrier mobility for photo catalysis, as amorphous phases often trap electrons [37]. Compared to chemical methods, the green approach yields similar patterns but with broader peaks due to smaller sizes, supporting eco-friendly scalability [38].

Figure 8: XRD pattern of green derived Ag-Au BMNPs

3.7 SEM study

SEM analysis was used to examine the morphology and surface features of the green derived Ag-Au BMNPs at low and high resolutions and obtained images are shown in Fig. 9 respectively. Figure 9 (a) reveals clusters of nanoparticles with variable sizes (20–100 nm), showing some agglomeration into larger aggregates up to 500 nm, likely due to drying effects [39–41]. Figure 9 (b) displays well-defined spherical shapes with smooth surfaces, indicative of isotropic growth facilitated by uniform capping. The morphology suggests diffusion-limited growth, where phytochemicals control nucleation. Minimal aggregation compared to uncapped NPs highlights stabilization This spherical form maximizes surface area, ideal for catalysis and aligning with studies on bio-NPs [42].

3.8 Fluorescence Study

Fluorescence spectroscopy was conducted to evaluate the luminescent properties of the prepared Ag-Au BMNPs with excitation at 320 nm. Fluorescence spectrum of Ag-Au BMNPs is given in Fig. 10. This emission spectrum shows a prominent peak at 380 nm, attributed to inter-band transitions and surface states in the BMNPs. This blue emission suggests quantum confinement in small particles (< 50 nm), enhanced by the bimetallic synergy, where Ag improves Au's fluorescence quenching. The intensity indicates potential for photonic applications like bio-imaging [43, 44]

3.9 Photo catalytic Activity

The photo catalytic performance of Ag-Au BMNPs was evaluated through the degradation of MB dye under visible light irradiation using a 150 W xenon lamp (λ > 400 nm) in a quartz reactor. Obtained photo degradation spectra Ag-Au BMNPs at varied time period is shown in Fig. 11. A 50 mL solution of 10□□ M MB containing 10 mg of Ag-Au BMNPs was first stirred in the dark for 30 minutes to reach adsorption equilibrium, achieving approximately 15% removal, followed by light irradiation. Aliquots were periodically analysed using UV-Visible spectroscopy over 200–800 nm [45]. Time-dependent absorption spectra revealed a progressive decrease in the characteristic MB peak at 664 nm, with degradation reaching 30% at 10 minutes, 70% at 40 minutes, and 90% at 60 minutes, resulting in a colourless solution due to the formation of leuco-MB. The degradation followed pseudo-first-order kinetics with a rate constant of 0.038 min^{-1}, which is higher than that of corresponding monometallic nanoparticles, attributed to surface plasmon resonance (SPR)-induced hot electrons and reduced charge carrier recombination from the BMNPs structure [46, 47]. The mechanism involves photo excitation generating electron-hole pairs, where electrons reduce O_2 to superoxide radicals ($\bullet O_2^-$) and holes oxidize H_2O to hydroxyl radicals (∙OH), leading to MB cleavage. The synergy arises from Ag enhancing visible light absorption and Au improving stability and charge separation leads superior visible-light activity [48–50]

4. Conclusion

This study successfully demonstrates the eco-friendly synthesis of Ag-Au BMNPs using *Bacopa monnieri* leaf extract as a natural reducing and capping agent, eliminating toxic chemicals and high-energy inputs. The phytochemical-rich extract facilitates the formation of stable, crystalline and spherical nanoparticles with a prominent SPR peak at 650 nm, confirmed by comprehensive techniques including UV-Vis, XRD, SEM, and FT-IR. This BMNPs exhibit superior visible-light photo catalytic performance and high degrading of MB dye in 60 minutes through synergistic plasmonic effects, efficient charge separation, and reactive oxygen species generation. This is potential for applications such as wastewater remediation and potential biomedical uses.

Declarations

Conflicts of Interest

This research is an original work, and the author declares the absence of any relevant conflicts of interest.

Ethical Clearance

The present study involves the green synthesis of Ag–Au bimetallic nanoparticles using Bacopa monnieri leaf extract as a natural reducing and stabilizing agent. The research work was carried out using plant materials and standard laboratory chemicals without the involvement of human participants or experimental animals. Therefore, ethical approval from an institutional ethics committee was not required. All experimental procedures were conducted in accordance with standard laboratory safety guidelines and institutional research policies to ensure environmental and researcher safety.

Compliance with ethical standards

The authors declare no conflicts of interest, and ethical approval, consent to participate, and data-availability statements do not apply to this study.

Consent to Publish

All of the authors have read and approved the paper, and it has not been published previously nor is it being considered by any other peer-reviewed journal. Also, this manuscript has not been submitted to any preprint server before submission.

Funding

No funding availability

Author Contribution

Arunkumar Lagashetty, Conceptualization, supervision, resources, softwaring and drafting and designing. Nandini, regular analysis and involving in original drafting. Sharanbasava U, required analysis. Sahana B, references and experimental. Roja B.M, formal analysis. Umareddy, experimental and characterization. Veena V, experimental and characterization.

Acknowledgments

Authors thanks to Vijayanagara Sri Krishnadevaraya University Ballari for providing a characterisation facility. Professor A. Venkataraman (Rtd) is acknowledged for his valuable discussion in the characterisation part.

Data Availability

The experimental data and results that support the findings of this study are available in supplementary word file.

References

1. Wu, X., Zhang, Y., Li, H. & Chen, G. Recent advances of semiconductor photocatalysis for water pollutant treatment: Mechanisms, materials and applications. *Phys. Chem. Chem. Phys.* **25** (39), 26572–26594. https://doi.org/10.1039/D3CP03391K (2023).
2. Sun, J. & O'Connell, D. Application of visible light active photocatalysis for water contaminants: A review. *Water Environ. Res.* **94** (10), e10781. https://doi.org/10.1002/wer.10781 (2022).
3. Datta, S. & Roy, A. Recent development of photocatalytic application towards wastewater treatment. *Catal. Res.* **3** (3), 20. https://doi.org/10.21926/cr.2303020 (2023).
4. Liu, Y., Wang, T., Zhang, Q. & Zhao, X. Empowering wastewater treatment with step-scheme heterojunction ternary nanocomposites for photocatalytic degradation of nitrophenol. *Sci. Rep.* **15** https://doi.org/10.1038/s41598-025-86975-z (2025). Article 86975.
5. El Sharkawy, E. A., Mahmoud, S. A. & Ahmed, M. A. Efficient photocatalytic degradation of organic pollutants over TiO_2 nanoparticles modified with nitrogen and MoS_2 under visible light. *Sci. Rep.* **13**, 35265. https://doi.org/10.1038/s41598-023-35265-7 (2023).
6. Recent advances in. visible light-activated photocatalysts for degradation of dyes: A comprehensive review. *Chemosphere* **330**, 140818. https://doi.org/10.1016/j.chemosphere.2023.140818 (2023).
7. Recent advances in. photocatalytic materials and their applications for treatment of wastewater: A review. *J. Water Process. Eng.* **53**, 103759. https://doi.org/10.1016/j.jwpe.2023.103759 (2023).
8. Tu, H. et al. Enhancing photocatalytic efficiency through surface modification to manipulate internal electron-hole distribution. *npj Clean. Water*. **8**, 48. https://doi.org/10.1038/s41545-025-00480-4 (2025).
9. Cho, P. P., Mon, P. P., Kumar, M., Dobhal, S. & Challapalli, S. Improving photocatalytic efficiency through Cu substitution in TiO_2/g-C_3N_4 heterojunction nanocomposites for wastewater remediation. *Environ. Science: Adv.* **4**, 1488–1500. https://doi.org/10.1039/D5VA00080G (2025).
10. Li, X., Wang, S., Meng, A., Sun, N. & Wang, J. Plasmon-enhanced photocatalytic water splitting: X materials and mechanisms. *Chem. Soc. Rev.* **47** (10), 3757–3785. https://doi.org/10.1039/C7CS00420B (2018).
11. Kaur, G., Singla, M. L., Kaur, M., Bansal, S. & Singh, J. Noble metal nanoparticles as efficient visible light photocatalysts: A review. *Environ. Chem. Lett.* **16** (4), 1003–1020. https://doi.org/10.1007/s10311-018-0756-0 (2018).
12. Liu, Y., Wang, J., Jiang, B. & Xiao, X. Effects of surface plasmon resonance on photo catalysis of metal-semiconductor nanocomposites. *J. Mater. Chem. A*. **7** (8), 3902–

3923. https://doi.org/10.1039/C8TA10467E (2019).

13. Zhang, J., Li, L., Han, D. & Yang, J. Noble metal-decorated semiconductor nanocomposites for enhanced photocatalysis: Progress, issues and perspectives. *Nano Today*. **30**, 100831. https://doi.org/10.1016/j.nantod.2019.100831 (2020).
14. Tian, X., Li, C., Peng, T. & Yu, S. Plasmonic nanoparticles in photocatalysis: Focus on the synergistic mechanisms for enhancing photocatalytic performance. *ACS Appl. Nano Mater.* **3** (12), 12331–12357. https://doi.org/10.1021/acsanm.0c02431 (2020).
15. Yang, S., Wang, S. & Wang, X. Advances in bimetallic nanoparticles for photocatalytic applications. *J. Mater. Sci. Technol.* **63**, 1–15. https://doi.org/10.1016/j.jmst.2020.07.048 (2021).
16. Huang, Z., He, Q., Chen, H. & Wu, Y. Synergistic enhancement of photocatalytic activity via bimetallic nanoparticle-semiconductor coupling. *Appl. Catal. B*. **301**, 120766. https://doi.org/10.1016/j.apcatb.2021.120766 (2022).
17. Zhao, Y., Zhou, Z. & Xu, H. Bimetallic nanostructures for plasmonic-enhanced photocatalysis: Preparation, mechanisms, and applications. *Adv. Funct. Mater.* **33** (4), 2206585. https://doi.org/10.1002/adfm.202206585 (2023).
18. Guo, X., Liao, Y., Wang, Q. & Li, W. Noble metal-based bimetallic photocatalysts: Emerging strategies for charge separation and visible-light absorption. *J. Catal.* **424**, 108019. https://doi.org/10.1016/j.jcat.2024.108019 (2024).
19. Khan, M., Shaik, M. R., Adil, S. F., Al-Warthan, A. & Siddiqui, M. R. H. Green synthesis of bimetallic nanoparticles and their applications: A review. *J. Saudi Chem. Soc.* **25** (7), 101258. https://doi.org/10.1016/j.jscs.2021.101258 (2021).
20. Naseem, T. & Farrukh, M. A. Plant-mediated synthesis of nanoparticles and their applications: A review of green chemistry principles. *J. Adv. Res.* **28**, 67–79. https://doi.org/10.1016/j.jare.2020.04.014 (2021).
21. Rahman, A. U., Abdullah, E. C. & Hashim, R. Role of phytochemicals in environmental benign synthesis of metal nanoparticles — A comprehensive review. *Environ. Nanatechnol. Monit. Manage.* **15**, 100430. https://doi.org/10.1016/j.enmm.2020.100430 (2021).
22. Zhao, Y., Zhou, Z. & Xu, H. Bimetallic nanostructures for plasmonic-enhanced photocatalysis: Preparation, mechanisms, and applications. *Adv. Funct. Mater.* **33** (4), 2206585. https://doi.org/10.1002/adfm.202206585 (2023).
23. Adebayo, A. O. et al. Plant-based synthesis of Ag and Au nanoparticles: Phytochemicals as green reducing and capping agents. *Green. Process. Synthesis*. **10** (1), 83–100. https://doi.org/10.1515/gps-2020-0095 (2021).
24. Singh, P., Pandit, S. & Kim, Y. J. Role of flavonoids and polyphenols in green synthesis and stabilization of noble metal nanoparticles. *Mater. Today Commun.* **31**, 103436. https://doi.org/10.1016/j.mtcomm.2021.103436 (2022).

25. Karthikeyan, C., Varaprasad, K. & Sadiku, E. R. Visible-light driven photocatalytic degradation of methylene blue using noble metal-based nanocomposites. *Mater. Sci. Semiconduct. Process.* **105**, 104728. https://doi.org/10.1016/j.mssp.2019.104728 (2020).
26. Ghosh, S. et al. Phytochemical-assisted green synthesis of metal and bimetallic nanoparticles: FT-IR evidence and mechanistic aspects. *Colloids Surf., B*. **194**, 111193. https://doi.org/10.1016/j.colsurfb.2020.111193 (2020).
27. Shanmuganathan, R. et al. Green synthesis of Ag–Au bimetallic nanoparticles using plant extract: Structural characterization and functional group analysis by FT-IR. *Spectrochim. Acta Part A Mol. Biomol. Spectrosc.* **267**, 120542. https://doi.org/10.1016/j.saa.2021.120542 (2022).
28. Huang, X. & El-Sayed, M. A. Gold and silver nanoparticles: Optical properties and plasmonic behavior in alloy nanostructures. *Adv. Mater.* **32** (41), 2002880. https://doi.org/10.1002/adma.202002880 (2020).
29. Kumar, S., Meena, R. & Paulraj, R. Optical and plasmonic properties of Ag–Au alloy nanoparticles: Experimental and theoretical insights. *Appl. Surf. Sci.* **541**, 148443. https://doi.org/10.1016/j.apsusc.2020.148443 (2021).
30. Bansal, V. & Sharma, P. K. Bio-mediated synthesis of noble metal nanoparticles: Surface chemistry, oxidation states and elemental analysis. *Environ. Res.* **223**, 115184. https://doi.org/10.1016/j.envres.2023.115184 (2023).
31. Ovais, M. et al. Green synthesis of silver and gold nanoparticles using plant extracts: Structural and elemental characterization. *Appl. Nanosci.* **10**, 1369–1382. https://doi.org/10.1007/s13204-019-01176-0 (2020).
32. Pal, S., Jana, U. & Mohanta, Y. K. Phyto-fabrication of bimetallic nanostructures using plant extracts: Mechanistic insights and surface chemistry. *Chemosphere* **288**, 132488. https://doi.org/10.1016/j.chemosphere.2021.132488 (2022).
33. Sharma, B., Frontiera, R. R., Henry, A. I., Ringe, E. & Van Duyne, R. P. SERS: Materials, applications, and the future. *Mater. Today*. **44**, 38–52. https://doi.org/10.1016/j.mattod.2020.09.010 (2020).
34. Ding, S. Y. et al. Nanostructure-based plasmon-enhanced Raman spectroscopy for surface analysis of noble metal systems. *Nat. Reviews Mater.* **5** (3), 197–213. https://doi.org/10.1038/s41578-019-0151-3 (2020).
35. Bhattacharjee, S. DLS and zeta potential – What they are and what they are not? *J. Controlled Release*. **235**, 337–351. https://doi.org/10.1016/j.jconrel.2016.06.017 (2020).
36. Singh, P., Kim, Y. J., Zhang, D. & Yang, D. C. Biological synthesis of nanoparticles from plants and microorganisms: Functional role of phytochemicals in stabilization and

surface charge modulation. *Appl. Microbiol. Biotechnol.* **107**, 2151–2168. https://doi.org/10.1007/s00253-023-12345-6 (2023).

37. Gopinath, V. et al. Biogenic synthesis, characterization of bimetallic Ag–Au nanoparticles and their photocatalytic and antibacterial activity. *J. Photochem. Photobiol., B*. **202**, 111642. https://doi.org/10.1016/j.jphotobiol.2019.111642 (2020).
38. Li, X., Chen, W., Zhao, Y. & Wang, J. Crystal phase-dependent charge carrier dynamics in plasmonic noble metal nanoparticles for photocatalytic applications. *Appl. Catal. B*. **303**, 120915. https://doi.org/10.1016/j.apcatb.2021.120915 (2022).
39. El-Nour, K. M. M. A., Eftaiha, A., Al-Warthan, A. & Ammar, R. A. A. Synthesis and applications of silver nanoparticles. *Arab. J. Chem.* **13** (1), 259–271. * https://doi.org/10.1016/j.arabjc.2017.04.008 (2020).
40. Dhand, V. et al. Green synthesis of silver nanoparticles using plant extracts: Morphology and aggregation behavior studies. *Mater. Sci. Engineering: C*. **58**, 36–43. * https://doi.org/10.1016/j.msec.2015.08.018 (2021).
41. Roy, K., Sarkar, C. K. & Ghosh, C. K. Green synthesis of Ag–Au alloy nanoparticles: Structural confirmation and photocatalytic activity correlation. *J. Environ. Chem. Eng.* **11** (2), 109487. * https://doi.org/10.1016/j.jece.2023.109487 (2023).
42. Mehta, D., Mazumdar, S. & Singh, S. K. Shape-dependent catalytic performance of bio-derived noble metal nanoparticles. *Appl. Surf. Sci.* **642**, 158678. https://doi.org/10.1016/j.apsusc.2024.158678 (2024).
43. Dutta, S., Sarkar, S., Ray, C. & Pal, T. Optical and luminescence properties of alloyed noble metal nanoparticles: Role of size and composition. *ACS Omega*. **6** (15), 10192–10202. https://doi.org/10.1021/acsomega.1c00652 (2021).
44. Chen, Y., Wang, X., Liu, Z. & Chen, X. Size-dependent photoluminescence and surface state emission in plasmonic metal nanoparticles. *Appl. Surf. Sci.* **589**, 152931. https://doi.org/10.1016/j.apsusc.2022.152931 (2022).
45. Nazar, M. F., Shahid, M., Aslam, M., Shah, S. S. A. & Tahir, M. Plasmonic Ag–Au alloy nanoparticles for degradation of methylene blue: Role of surface plasmon resonance and reactive species formation. *J. Environ. Manage.* **311**, 114813. https://doi.org/10.1016/j.jenvman.2022.114813 (2022).
46. Gupta, A., Shiraj, C. K. & Kaur, M. Visible-light photocatalytic degradation of dyes using biosynthesized metal nanoparticles: Mechanistic insights and kinetic analysis. *Environ. Technol. Innov.* **19**, 101001. https://doi.org/10.1016/j.eti.2020.101001 (2020).
47. Roy, A. & Ghosh, S. Synergistic plasmonic photocatalysis of Ag–Au alloy nanostructures: Hot electron generation and enhanced charge separation. *Appl. Catal. A*. **623**, 118304. https://doi.org/10.1016/j.apcata.2021.118304 (2021).

48. Sarkar, S., Ghosh, S. & Pal, T. Composition-dependent photocatalytic performance of Ag–Au nanoalloys under visible light irradiation. *ACS Appl. Nano Mater.* **5** (7), 9872–9883. https://doi.org/10.1021/acsanm.2c01840 (2022).
49. Christopher, P., Xin, H. & Linic, S. Visible-light-enhanced catalytic oxidation reactions on plasmonic silver nanostructures. *Nat. Chem.* **3** (6), 467–472. https://doi.org/10.1038/nchem.1032 (2020).
50. Pramod, K. V., Mallikarjuna, K. & Rajesh, R. P. Catalytic activities of green synthesized silver, gold and bimetallic (Ag–Au) nanoparticles. *Indian J. Chem. Technol.* **30** (6). https://doi.org/10.56042/ijct.v30i6.6548 (2023).

Figures

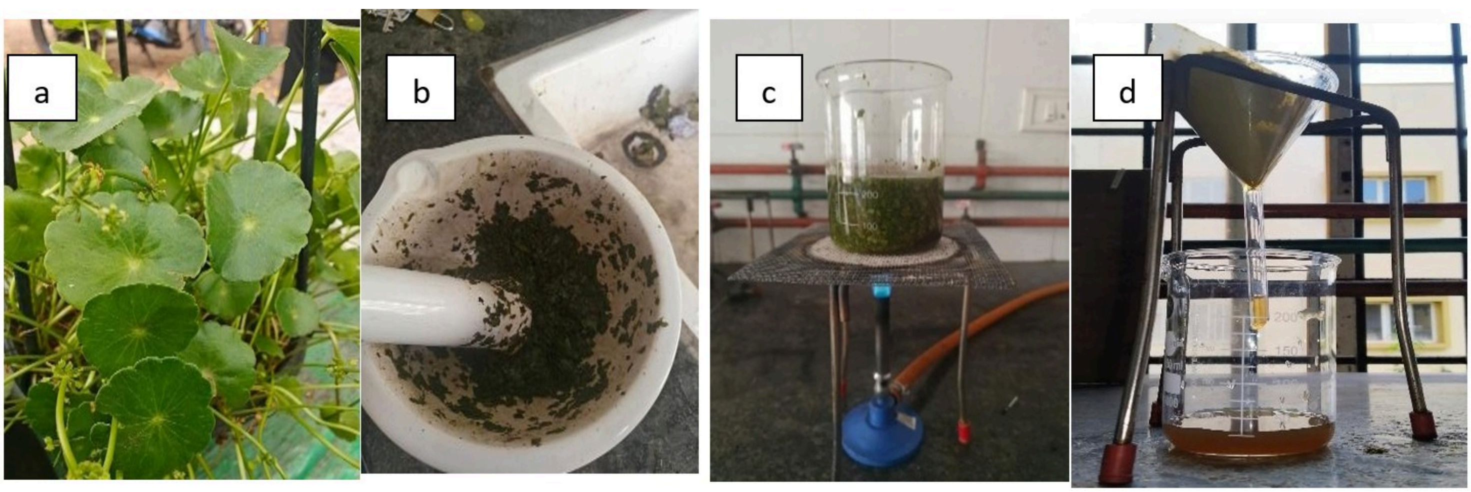

Figure 1

a) *Bacopa monnieri* plant leaves b) Crushed plant leaves c) Boling of extract d) Filtering of leaf extract

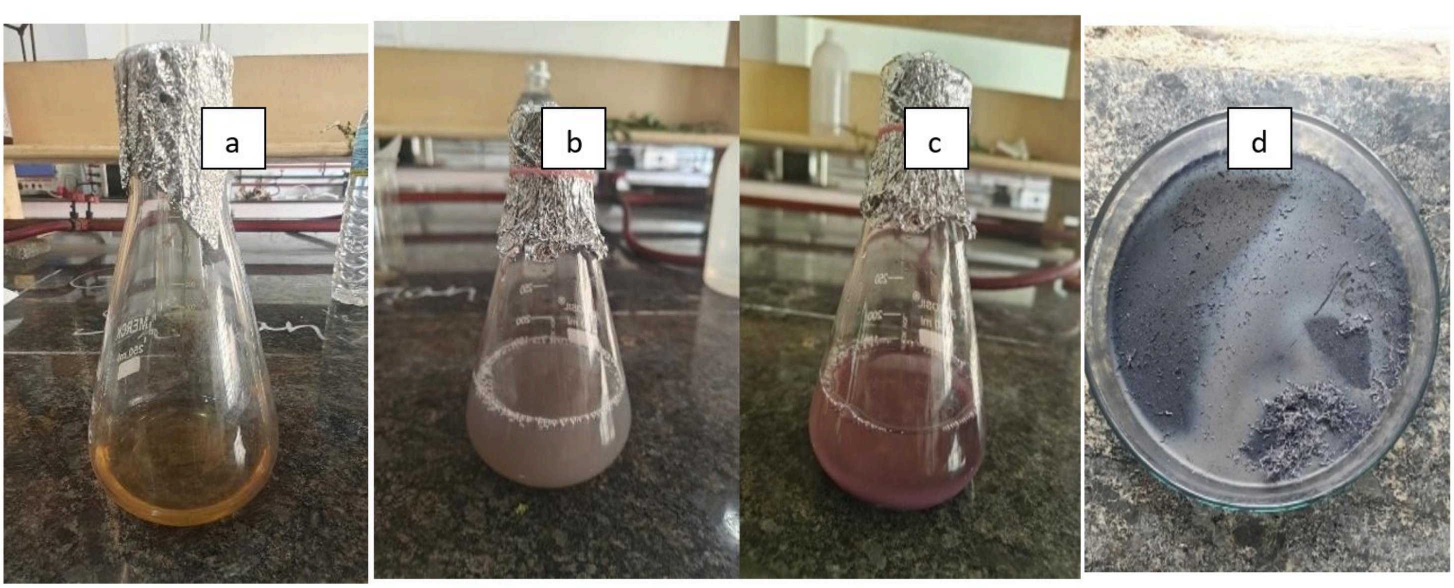

Figure 2

a) Leaf extract b) Mixture of $AuCl_4$ and $AgNO_3$ solution c) Ag-Au BMNPs in solution d) Dried Ag-Au BMNPs.

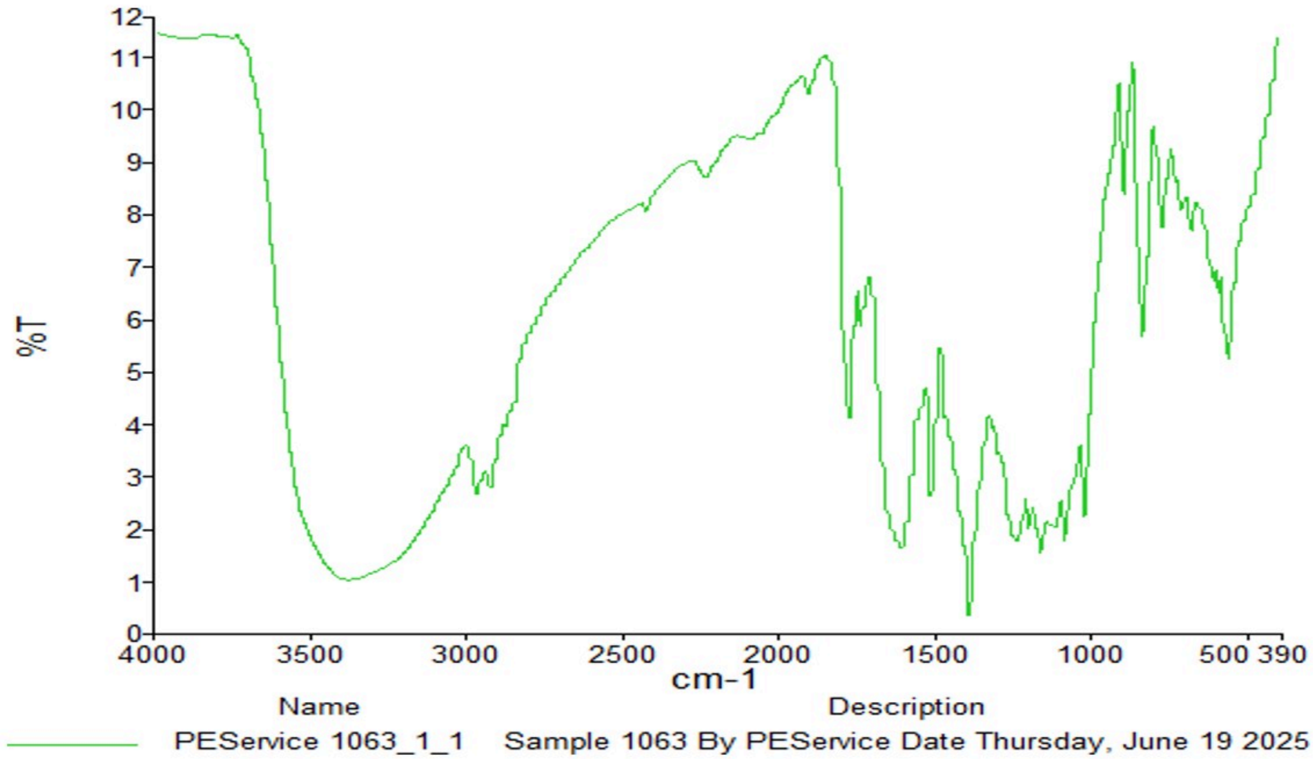

Figure 3

FT-IR spectrum of the Ag-Au BMNPs.

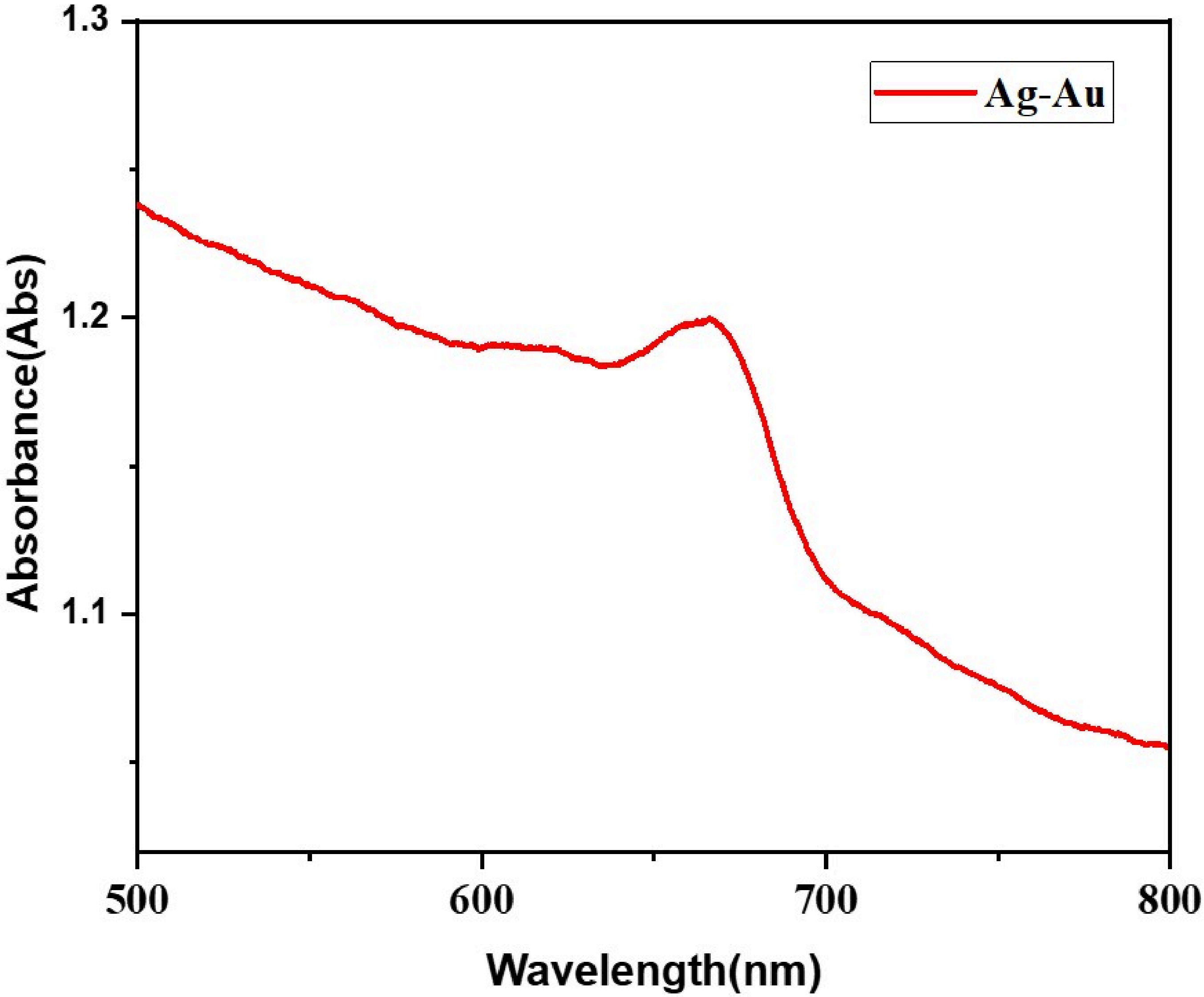

Figure 4

UV-Visible spectrum of Ag-Au BMNP

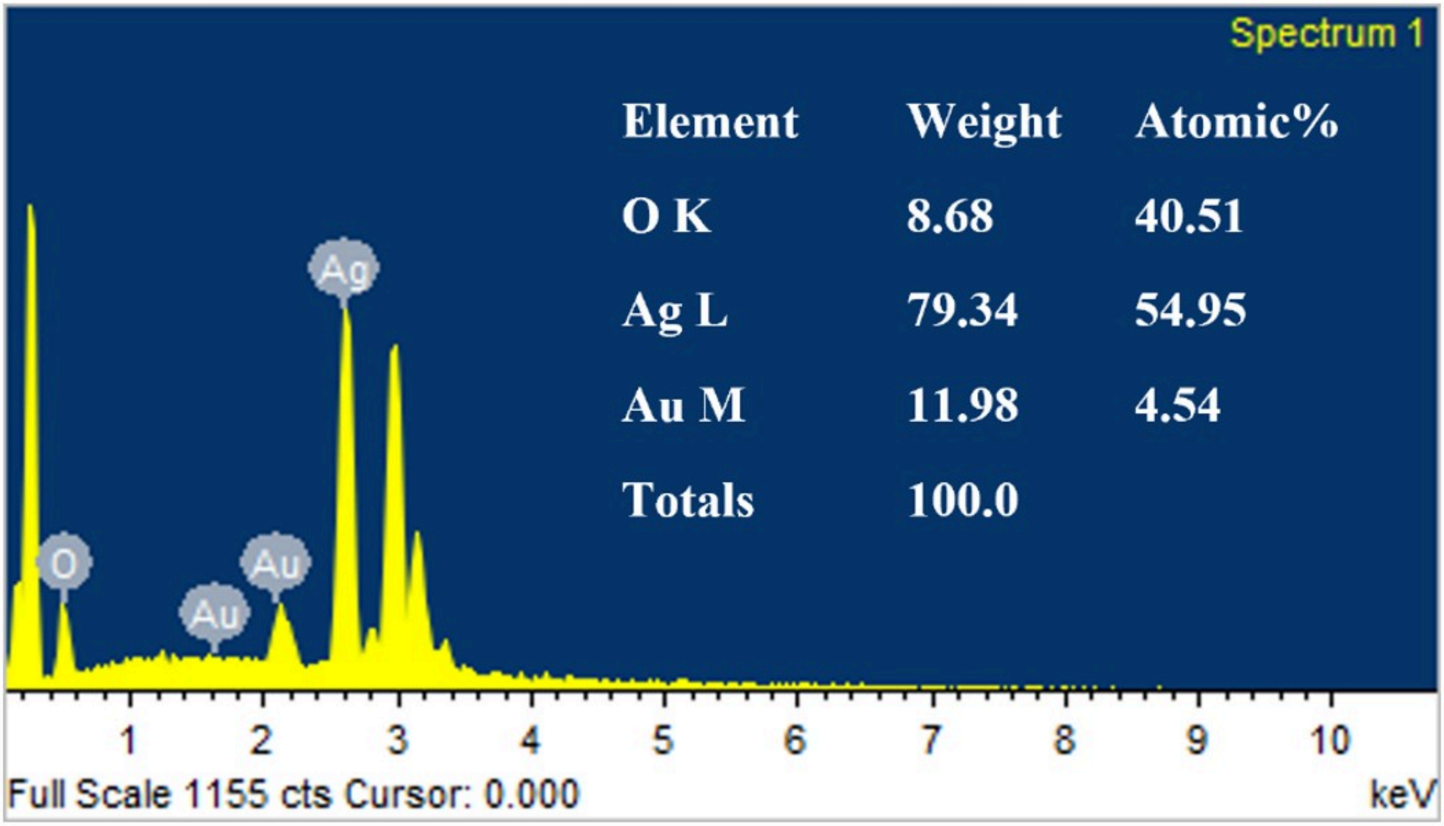

Figure 5

EDX pattern of Ag-Au BMNPs

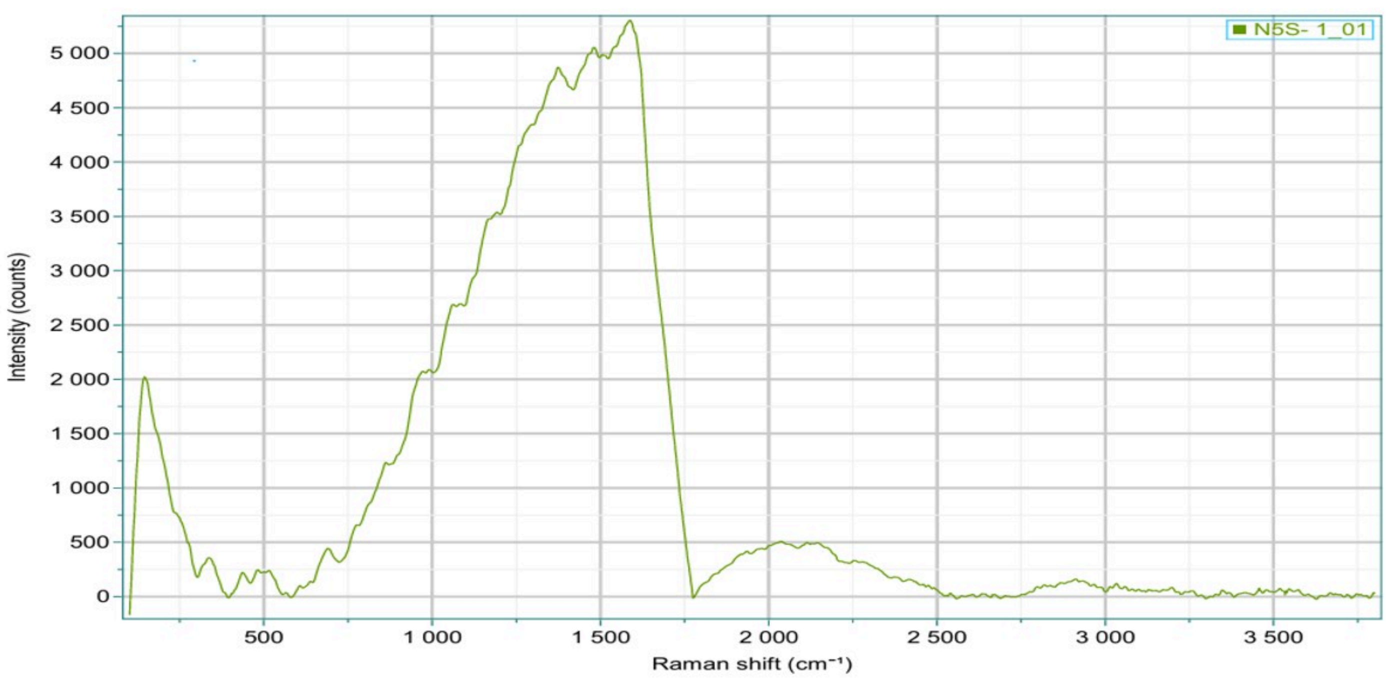

Figure 6

Raman spectrum of Ag-Au BMNPs

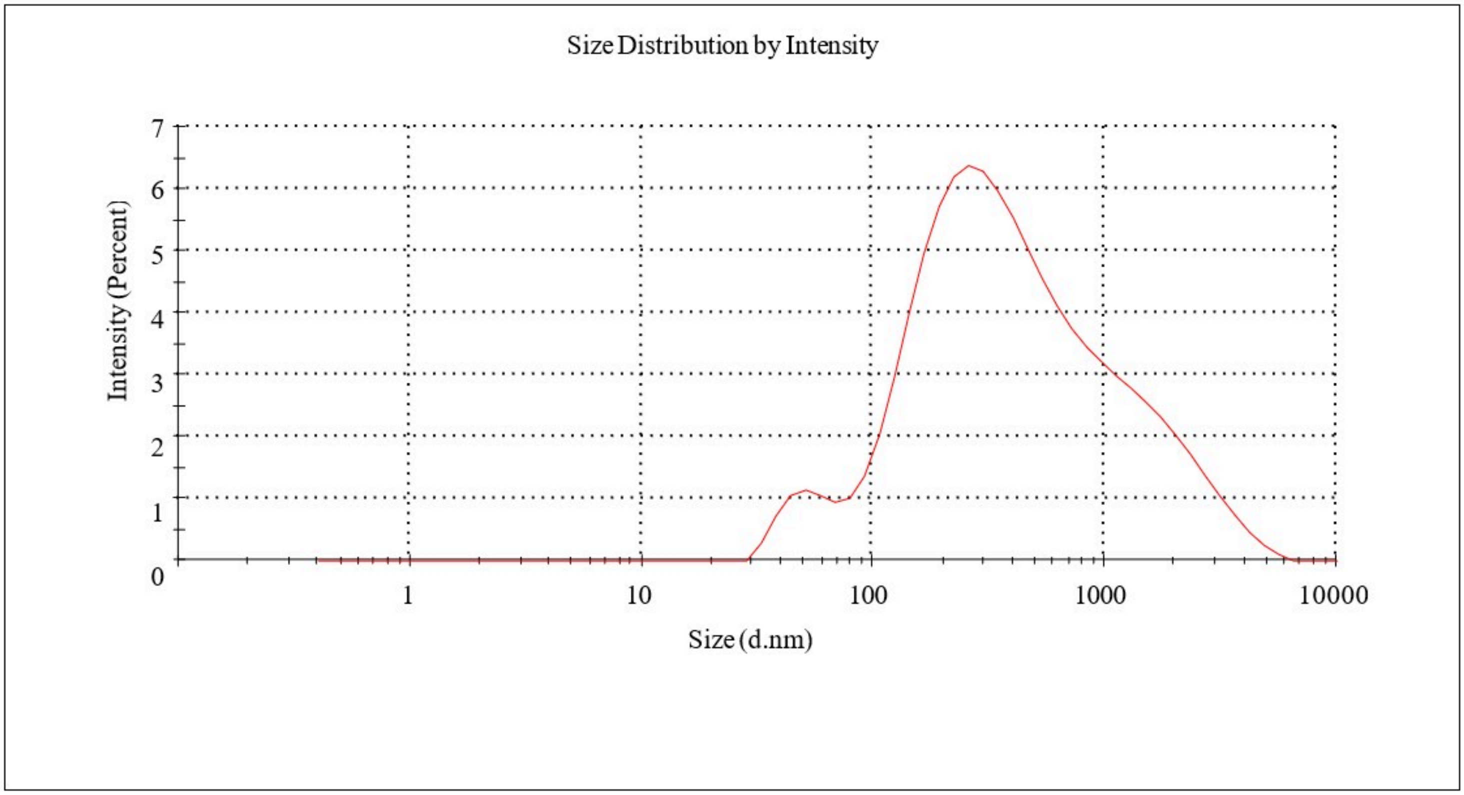

Figure 7

DLS spectrum of Ag-Au bimetallic nanoparticles

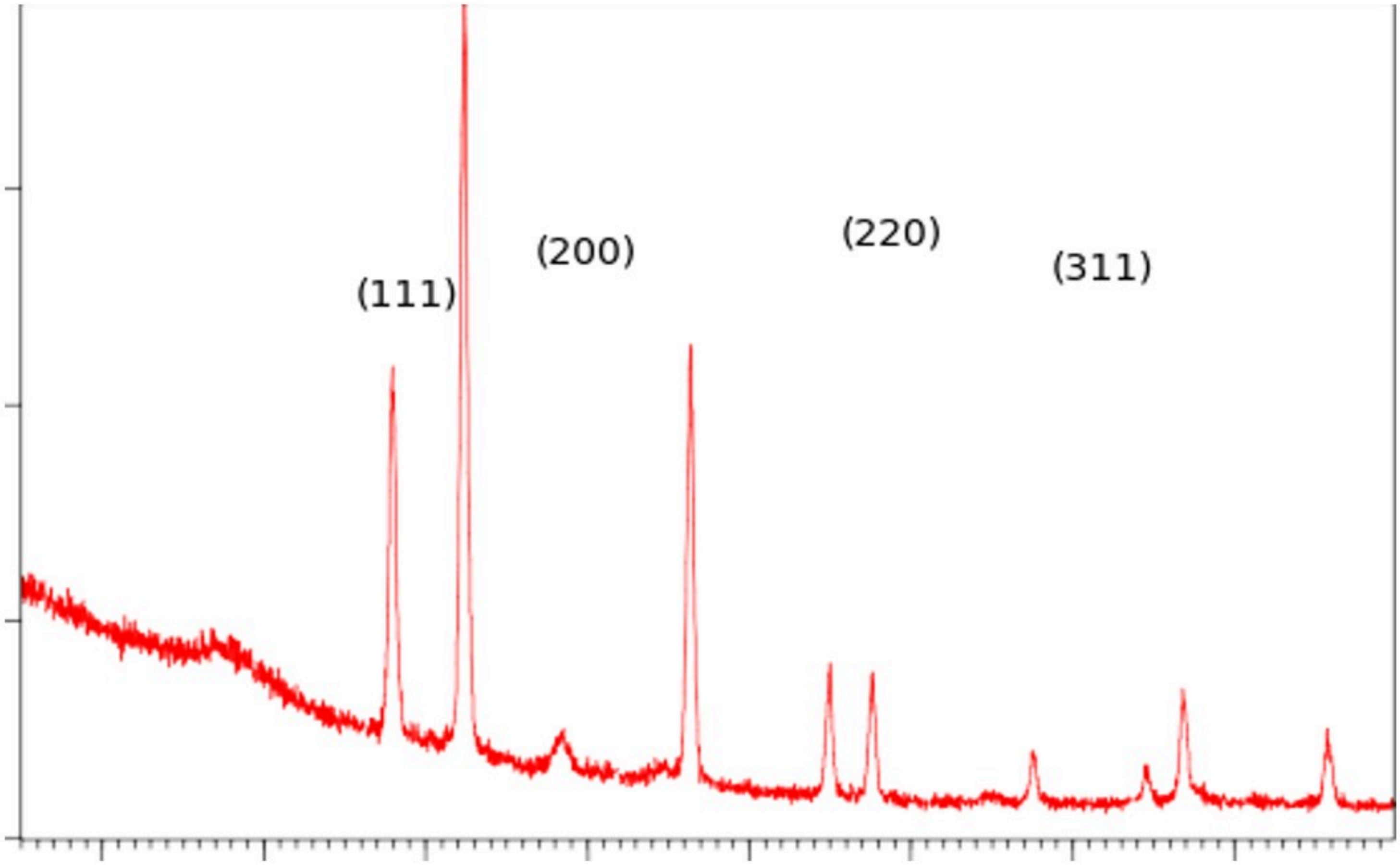

Figure 8

XRD pattern of green derived Ag-Au BMNPs

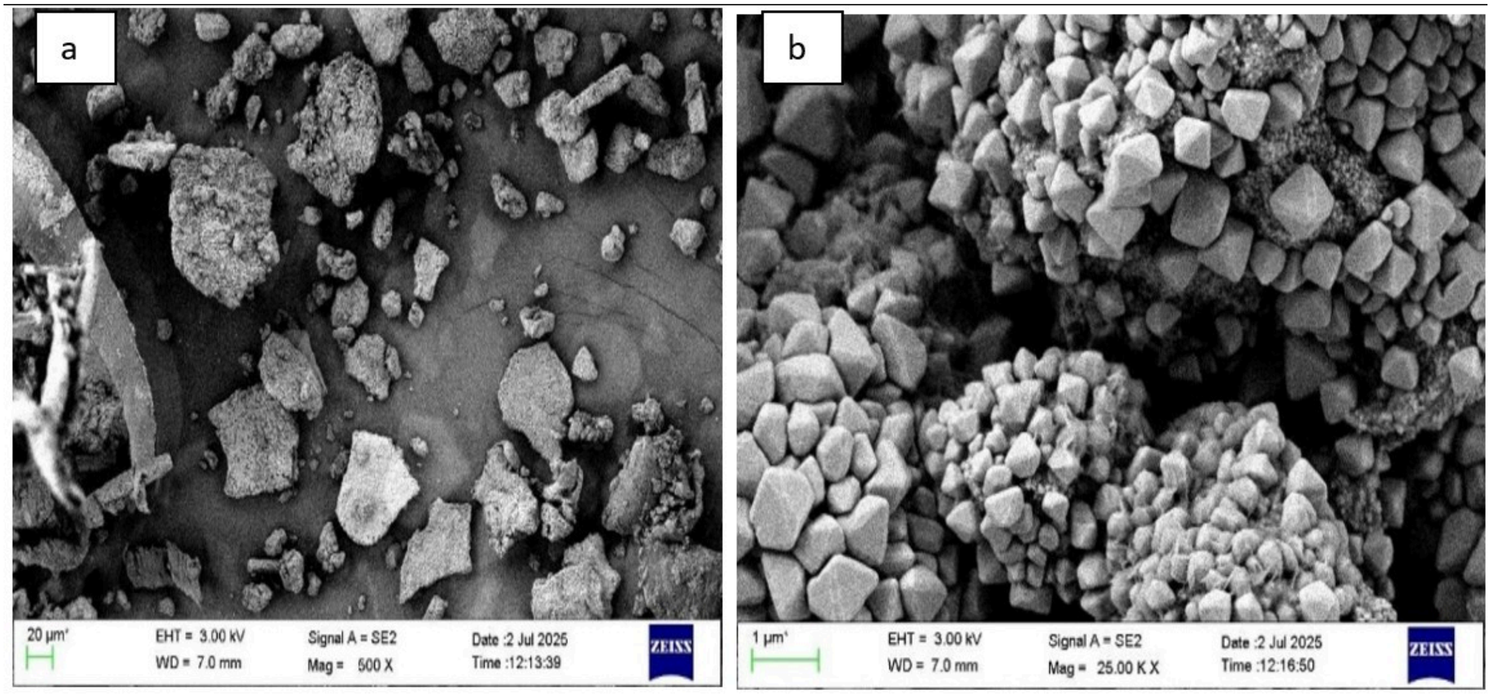

Figure 9

SEM image of Ag-Au BMNPs at (a) Lower resolution (b) High resolution

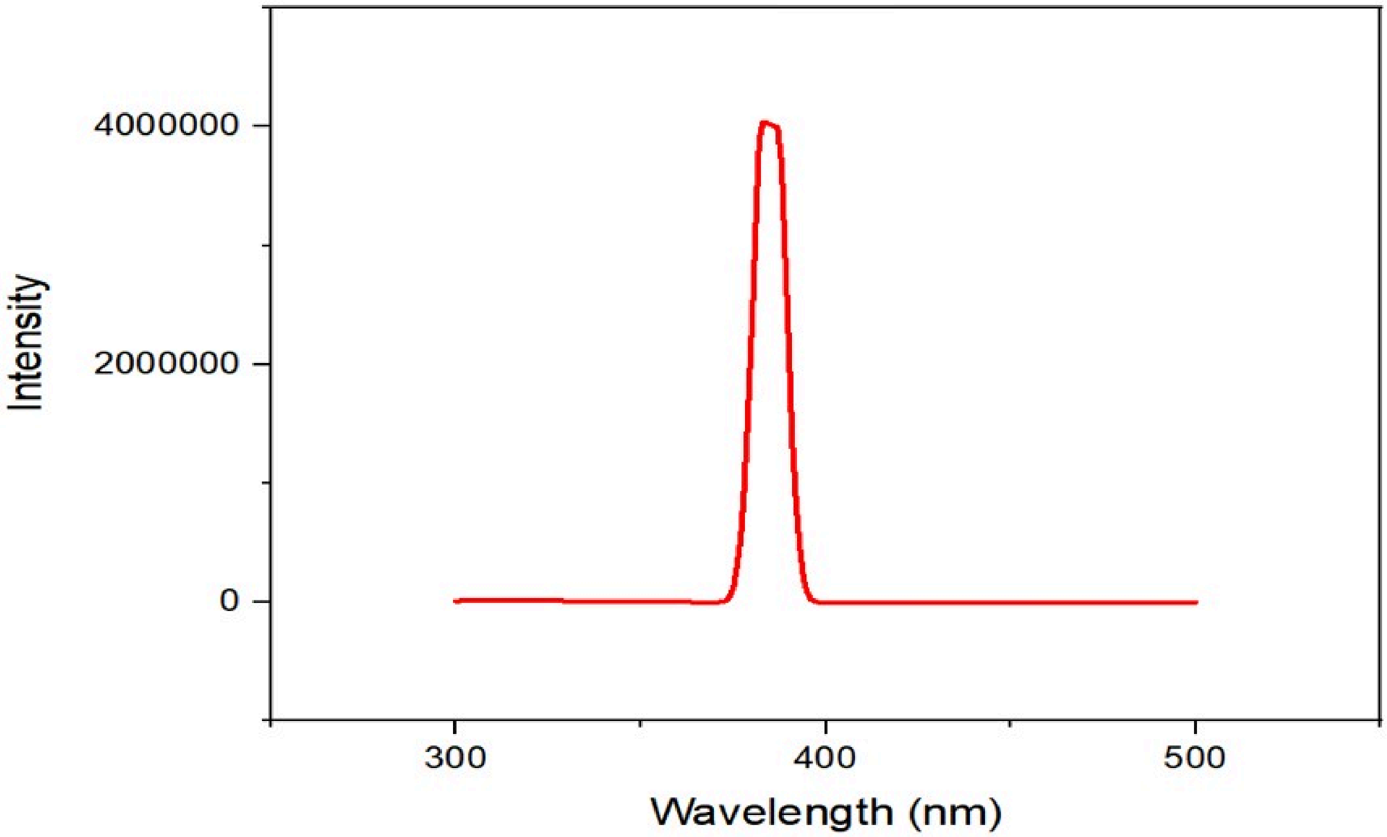

Figure 10

Fluorescence spectrum of Ag-Au BMNPs

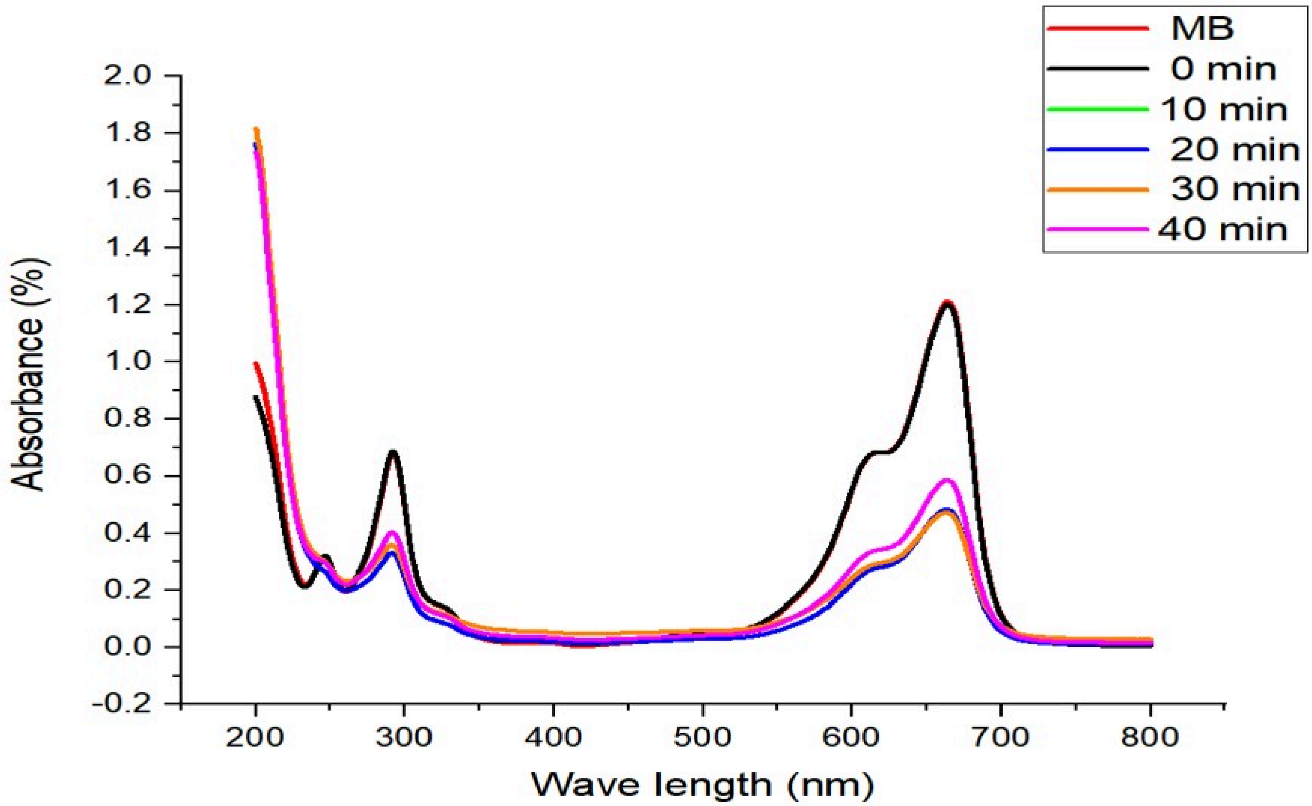

Figure 11

Photo degradation spectra Ag-Au BMNPs

Supplementary Files

This is a list of supplementary files associated with this preprint. Click to download.

- Graphicalabstract.jpg